# A global view of horizontally oriented crystals in ice clouds from Cloud-Aerosol Lidar and Infrared Pathfinder Satellite Observation (CALIPSO)

Vincent Noel, Hélène Chepfer

▶ **To cite this version:**

Vincent Noel, Hélène Chepfer. A global view of horizontally oriented crystals in ice clouds from Cloud-Aerosol Lidar and Infrared Pathfinder Satellite Observation (CALIPSO). Journal of Geophysical Research: Atmospheres, 2010, 115 (10), pp.D00H23. 10.1029/2009JD012365 . hal-01135807

**HAL Id: hal-01135807**
**https://hal.science/hal-01135807**

Submitted on 25 Mar 2015

**HAL** is a multi-disciplinary open access archive for the deposit and dissemination of scientific research documents, whether they are published or not. The documents may come from teaching and research institutions in France or abroad, or from public or private research centers.

L'archive ouverte pluridisciplinaire **HAL**, est destinée au dépôt et à la diffusion de documents scientifiques de niveau recherche, publiés ou non, émanant des établissements d'enseignement et de recherche français ou étrangers, des laboratoires publics ou privés.

JOURNAL OF GEOPHYSICAL RESEARCH, VOL. 115, D00H23, doi:10.1029/2009JD012365, 2010

Click Here for Full Article

# A global view of horizontally oriented crystals in ice clouds from Cloud-Aerosol Lidar and Infrared Pathfinder Satellite Observation (CALIPSO)

Vincent Noel[1] and Helene Chepfer[2]

Received 30 April 2009; revised 19 December 2009; accepted 31 December 2009; published 26 May 2010.

[1] We analyze optical signatures in 18 months of CALIOP layer-integrated backscatter and depolarization ratio to investigate the geographical and seasonal distribution of oriented crystals in ice clouds on a global scale. Oriented crystals are found to be rare: they appear in ~6% of all ice cloud layers, and inside these layers the proportion of oriented crystals is estimated below 5%, even though they have a significant effect on the cloud optical properties. The geographical pattern of crystal orientation is very stable over the year, without any noticeable cycle. We investigate the atmospheric conditions which might lead to crystal orientation, including synoptic-scale dynamics and thermodynamic profiles. In the tropics, detections of crystal orientation are more numerous in areas dominated by convection on a monthly basis, and at midlatitudes less numerous in areas dominated by strong horizontal winds. Synoptic effects, however, appear secondary; orientation is primarily driven by temperature. Oriented crystals are mostly nonexistent in ice clouds colder than −30°C, and very frequent in warmer ice clouds, appearing in 30% of such clouds in the tropics and up to 50% at higher latitudes. The temperatures where oriented crystals are found (−30°C to −10°C) are conducive to the formation of planar crystals. Results suggest oriented crystals are more frequent just above cloud base in slightly thicker cloud layers, which might provide clues to how and why orientation takes place.

**Citation:** Noel, V., and H. Chepfer (2010), A global view of horizontally oriented crystals in ice clouds from Cloud-Aerosol Lidar and Infrared Pathfinder Satellite Observation (CALIPSO), *J. Geophys. Res.*, *115*, D00H23, doi:10.1029/2009JD012365.

## 1. Introduction

[2] Under specific circumstances, crystals in ice clouds can orient themselves horizontally [*Sassen*, 1980], generating unusual optical displays [*Lynch et al.*, 1994]. If the crystals present plane-parallel faces, horizontal orientation creates very strong specular reflections [*Yang et al.*, 2003] which increase cloud albedo by as much as 40% compared to randomly oriented crystals according to light scattering models [*Takano and Liou*, 1989]. This phenomenon could therefore have consequences on the local or global radiative impact of ice clouds. It also affects instruments [*Lavigne et al.*, 2008], leading to important bias when retrieving cloud optical properties [*Masuda and Ishimoto*, 2004]. Moreover, crystal orientation impacts sedimentation speed [*Heymsfield and Iaquinta*, 2000; *Westbrook*, 2008], which affects cloud lifetime and persistence in atmospheric models [*Spichtinger and Gierens*, 2009]. We thus need to progress in our understanding of this phenomena: quantify the global spatiotemporal distribution of horizontally oriented crystals and the amount of crystal that orient themselves preferentially, understand what thermodynamic conditions drive orientation and explore possible links between oriented crystals and large-scale dynamics.

[3] Crystal orientation depends heavily on particle shape [*Klett*, 1995]. It is generally assumed that ice crystals presenting plane-parallel faces, such as planar or columnar crystals, have a higher chance of orienting themselves horizontally; horizontal faces result in specular reflection and slower sedimentation. It is sometimes argued that nonplanar crystal shapes such as bullet rosettes can also adopt a preferential orientation [*Evans et al.*, 1998]; however such crystals present less plane-parallel faces, thus have a smaller impact on light-cloud interaction (e.g., no specular reflection) and sedimentation speeds. To the knowledge of the authors there has been no attempt to detect oriented nonplanar crystals through remote sensing. Most observation studies have focused on planar and columnar crystals, and so will this one.

[4] Crystal orientation is hard to detect. Direct in situ observation is impossible since the intense turbulence created by aircraft flight temporarily destroys preferential orientation, so studies have to rely on its optical effects. Remote sensing requires observations that describe aniso-

[1]Laboratoire de Météorologie Dynamique, IPSL, Ecole Polytechnique, CNRS, Palaiseau, France.
[2]Laboratoire de Météorologie Dynamique, IPSL, Université Paris 6, Paris, France.

Copyright 2010 by the American Geophysical Union.
0148-0227/10/2009JD012365

tropic optical properties [*Mishchenko et al.*, 1997], which are rare. Ground-based lidar instruments, with fixed [*Platt et al.*, 1978; *Sassen*, 1980] or scanning line of view [*Sassen and Takano*, 2000; *Noel and Sassen*, 2005] have provided most of the case studies of oriented crystals, but their local results cannot be extended to the global scale. Among spaceborne instruments, multiangular measurements from the Polarization and Directionality of the Earth Reflectances (POLDER-1) instrument have been successfully used to detect horizontally oriented plates [*Chepfer et al.*, 1999; *Bréon and Dubrulle*, 2004; *Noel and Chepfer*, 2004]. The signature of elusive vertically oriented crystals was also found by *Prigent et al.* [2005] in measurements from the Tropical Rainfall Measuring Mission (TRMM). Due to this difficult detection, the reasons as to how and why oriented crystals are distributed in space and time remain largely unknown.

[5] The Cloud-Aerosol Lidar with Orthogonal Polarization (CALIOP) orbits Earth roughly 14 times a day on the Cloud-Aerosol Lidar and Infrared Pathfinder Satellite Observation (CALIPSO) platform, part of the A-Train constellation. During the first 18 months of operation, CALIOP pointed 0.3° away from geodetic nadir in the forward along-track direction, to avoid specular lidar returns from still water [*Winker et al.*, 2007]. However, a review of the obtained data showed that, at this angle, specular returns from oriented crystals in ice clouds introduced biases of unexpected magnitude in the retrieval of optical properties for the affected cloud layers. To avoid these effect, the off-nadir angle was permanently increased to 3° in November 2007 after two test periods. Subsequent studies showed that at 0.3°, the presence of oriented crystals in a cloud layer produces atypical values of layer-integrated attenuated backscatter and depolarization ratio [*Hu et al.*, 2007; *Cho et al.*, 2008]. The present study applies this knowledge to infer the frequency of oriented crystals in clouds from CALIOP 0.3° off-nadir observations, with the objectives to understand (1) their seasonal and geographical global distribution and (2) how thermodynamical atmospheric conditions affect preferential orientation at both synoptic and local scales. Due to the limitations of lidar penetration in thicker clouds, results of the present study will be mostly representative of optically thin clouds.

[6] The CALIOP observations used in the present study are presented in section 2, along with the algorithm used to detect the presence of oriented crystals in clouds. We then expose the retrieved properties of oriented crystals, focusing first on their concentration (section 3), second on their vertical distribution–temperature and position within the cloud (section 4), and finally on their geographic/seasonal distribution and relationship with synoptic-scale dynamic indicators (section 5). Findings are discussed in section 6.

## 2. Detecting Horizontally Oriented Particles in Cloud Layers

### 2.1. Cloud Layers

[7] From CALIOP's initial laser shot on 7 June 2006 to the definitive off-nadir angle change on 27 November 2007, approximately 18 months of CALIOP data were recorded at 0.3° off-nadir angle. The whole data set for this period has been considered in the present study, excluding the 3° off-nadir angle test periods (7 November to 17 November 2006 and 21 August to 7 September 2007). Following recent CALIOP analyses [e.g., *Pitts et al.*, 2007; *Noel et al.*, 2008], only nighttime observations were considered since they are less affected by instrumental bias and provide better signal-to-noise ratio, amounting to a little more than 6700 half orbits or 25 millions profiles over the considered period. The period from June to November is better sampled (700 to 800 half orbits per month) than the rest of the year (350 to 400), with December 2006 being the least sampled month with two missing observation weeks due to satellite issues (252 half orbits).

[8] The CALIOP level 2 Cloud Product describes cloud physical properties [*Vaughan et al.*, 2005] after atmospheric layers were detected in level 1 data and identified as clouds using an adaptive threshold on the magnitude and spectral variation of lidar backscatter [*Vaughan et al.*, 2004]. The present study uses the following level 2 data: cloud base and top altitudes, layer-integrated attenuated backscatter, volume depolarization and color ratios. The granularity of cloud altitudes in level 2 data depend on the level 1 data resolution, 30 m for layers below 8.2 km and 60 m above; hence, in the rest of the paper, the term ≪cloud layer≫ will describe a slice of atmosphere at least 5 km long and 30 m tall identified by its optical properties as a cloud by the CALIOP level 2 algorithms. The cloud midlayer temperature and the tropopause altitude were also used, both included in level 2 data files and provided by NASA's Global Modeling and Assimilation Office using the Goddard Earth Observing System Model 5 model (GEOS-5). Finally, we also used the level 2 layer opacity flag which describes if there is still signal backscattered below a layer by searching for the ground return. Its absence means the lidar laser beam was totally attenuated while penetrating the last described layer, hence it is impossible to be sure if that layer was probed down to its base.

[9] Level 2 data contains the CALIOP thermodynamical phase flag, which identifies a cloud as either liquid water or ice [*Liu et al.*, 2005]. However, at the time of writing, the algorithm did not take into account oriented crystals, meaning their presence often leads to misclassification. Because of this, the level 2 cloud phase flag was not used here. Instead, ice clouds were identified using values of layer-integrated backscatter and depolarization as explained in the next section.

### 2.2. Ice Clouds and Horizontally Oriented Crystals

[10] In a first step, cloud layers were filtered according to several criteria. In order to consider only tropospheric clouds and remove any instance of stratospheric layers from the data set, layers with top higher than 1 km above the tropopause level were discarded. Obviously incorrect layer-integrated values were also filtered out to account for any possible instrumental problem. Opaque layers (based on the opacity flag, section 2.1) were also discarded, as such layers might not be entirely probed by the lidar, thus leading to nonrepresentative observations.

[11] The distribution of layer-integrated total attenuated backscatter and volume depolarization ratio for the remaining cloud layers, normalized by the entire number of profiles for each data set, is shown in Figures 1a and 1c, using a logarithmic color scale and bin sizes of 0.01 for

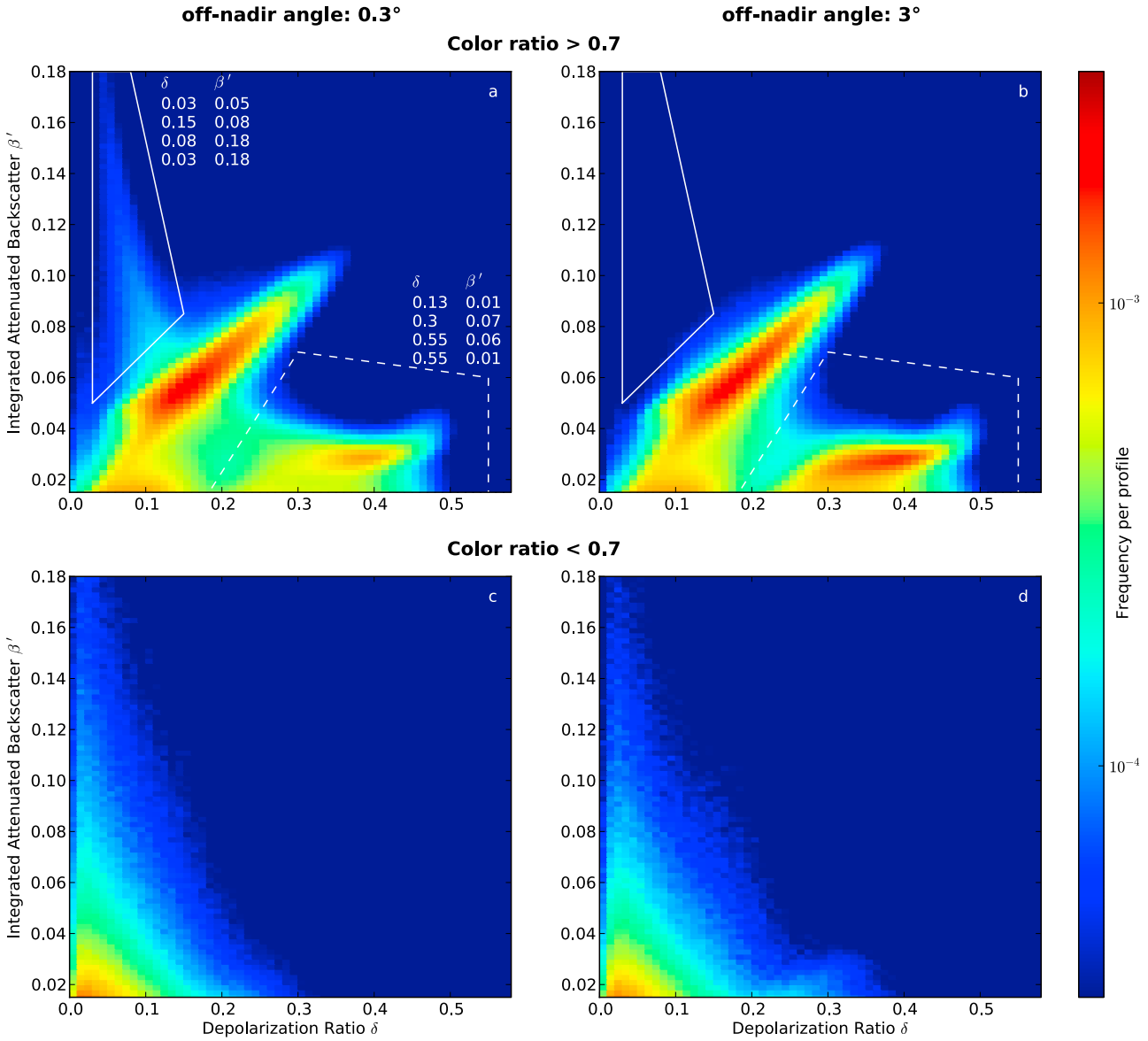


**Figure 1.** Distributions of integrated attenuated backscatter and depolarization ratio in layers identified as clouds with cloud top at most 1 km below the tropopause, and integrated color ratios (a and b) above 0.7 and (c and d) below 0.7, observed with an off-nadir angle of 0.3° (Figures 1a and 1c, June 2006 to November 2007) and 3° (Figures 1b and 1d, December 2007 to July 2008). The upper left arc (full outline) is symptomatic of oriented crystals, and the bottom right arc (dashed outline) indicates ice. Figure 1a lists the coordinates of the polygons bounding each arc.

depolarization ratio and 2 $10^{-3}$ $km^{-1}$ $sr^{-1}$ for attenuated backscatter. This data set was split into 2 categories according to the layer-integrated color ratio CR: high CR (above 0.7, Figures 1a and 1b) correspond to cloud particles, while low CR (below 0.7, Figures 1c and 1d) correspond to smaller particle sizes. Many layers identified as clouds in CALIOP Level 2 data produce CR < 0.7, associated distributions of integrated backscatter and depolarization ratio are centered on zero (Figure 1c). The actual nature of particles in these layers is uncertain at this stage, possible candidates include $H_2SO_4$-based [*Bogdan et al.*, 2006] or very small, near-spherical ice particles (e.g., from contrails [*Immler et al.*, 2008]) potentially containing $HNO_3$ [*Chepfer and Noel*, 2009]. Since CR below 0.7 cannot be understood as typical ice clouds [*Beyerle et al.*, 2001], in the rest of the present analysis we will only consider cloud layers with integrated CR above 0.7 (Figures 1a and 1b).

[12] Figure 1a closely reproduces results from *Cho et al.* [2008], who attributed the diagonal arc to water clouds (depolarization increasing linearly with integrated backscatter due to multiple scattering) and the bottom right arc to regular ice clouds (uniform low backscatter and strong depolarization in the 0.2–0.5 range). *Hu et al.* [2007] attributed the upper left arc to oriented ice crystals, as

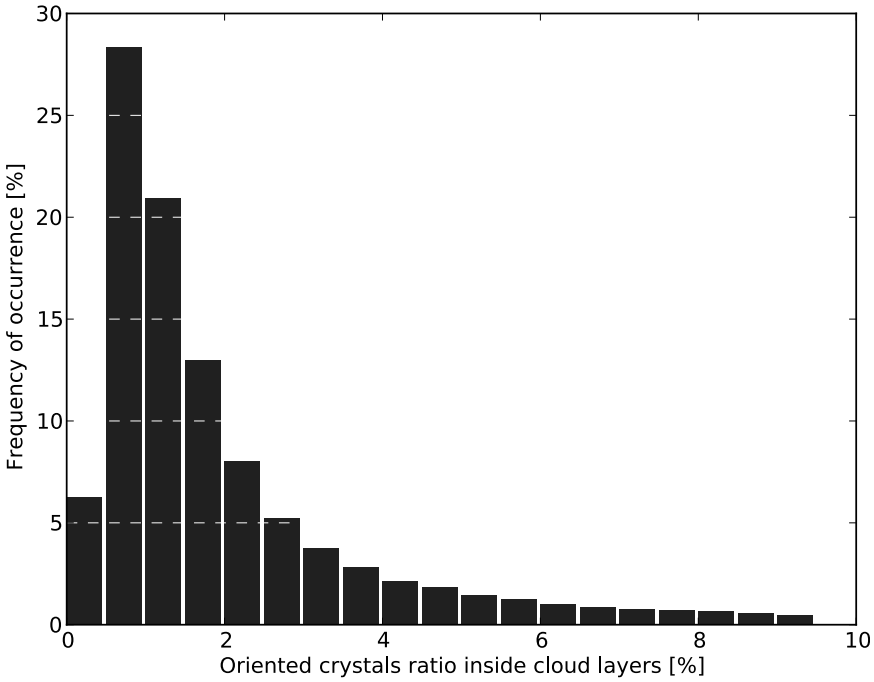


**Figure 2.** Distribution of the ratio of horizontally oriented particles on randomly oriented particles inside cloud layers identified as containing oriented particles for 0.3° off-nadir observations (June 2006 to November 2007).

very low depolarization and strong backscatter (full outline in Figure 1a) are typical of oriented planar or columnar crystals [*Noel and Sassen*, 2005]. The full outline in Figure 1a contains ~2.7% of all cloud layers and ~6.6% of ice clouds. For comparison purposes, the same distribution for CALIOP 3° off-nadir observations (27 November 2007 to 31 December 2008) is shown in Figures 1b and 1d. In Figure 1b, the upper left arc attributed to oriented crystals has almost entirely disappeared but still describes ~0.6% of all cloud layers; it is not surprising that the signature of oriented crystals is still faintly present even at 3° off-nadir since these crystals can wobble around the horizontal axis with sometimes wide angles (up to 10° [*Noel et al.*, 2002]). It is interesting to notice that the lower right arc, attributed to ice clouds, is more pronounced than in 0.3° off-nadir observations; it can be suggested that the ice clouds composed of oriented crystals, that previously composed the upper left arc which has now disappeared, are now part of this arc. For layers with CR < 0.7, the distribution is almost not affected by the off-nadir angle change (Figures 1c and 1d), it confirms they do not contain oriented particles and can be ignored here.

[13] Following these results: (1) ice clouds were identified by requiring layer-integrated total attenuated backscatter and volume depolarization ratio to be part of either the upper left or bottom right (solid and dashed outlined areas, respectively, in Figure 1a). Approximately 98% of clouds colder than −50°C satisfy this requirement; it seems thus reasonable to assume this scheme correctly identifies most ice clouds. This scheme, which is similar to the next iteration of the CALIOP phase discrimination algorithm [*Hu et al.*, 2009], classifies ~4% of clouds warmer than 0°C as ice clouds; as the number of liquid water clouds decreases with colder temperatures this bias should quickly get negligible. Misclassifications could be due to bias in temperatures reported by the GEOS-5 model, which might not be able to reproduce temperature variations at the CALIOP observation scale [*Noel et al.*, 2009]. It should also be noted that mixed-phase clouds with no oriented crystals would most probably end up at the juncture of the bottom right ice cloud arc and the diagonal liquid water cloud arc in Figure 1a. These clouds will not be considered in the present study. (2) The presence of oriented crystals was identified in cloud layers by requiring layer-integrated total attenuated backscatter and volume depolarization ratio to be part of the upper left arc (fully outlined area in Figures 1a and 1b). This means oriented crystals are detected for depolarization ratios below 0.12 (Figure 1a), which according to *Sassen and Benson* [2001] translates to at least one horizontally oriented crystal for ~154 randomly oriented crystals (i.e., less than 1%; see section 3).

## 3. Amount of Oriented Crystals

[14] *Sassen and Benson* [2001] present a formula to estimate the variability of the depolarization ratio in the presence of oriented crystals, as a function of the number of oriented crystals $n_h$ on the number of randomly oriented crystals $n_r$. From this formula, the ratio $\frac{n_h}{n_r}$ can be expressed as a function of the depolarization ratio produced by horizontally oriented particles $\delta$:

$$\frac{n_h}{n_r} = \left(\frac{\delta_r}{\delta} - 1\right)\frac{\beta_r}{\beta_h} \tag{1}$$

with $\delta_r$ the depolarization ratio the same particles would produce if randomly oriented, and $\beta_r$ and $\beta_h$ the backscatter

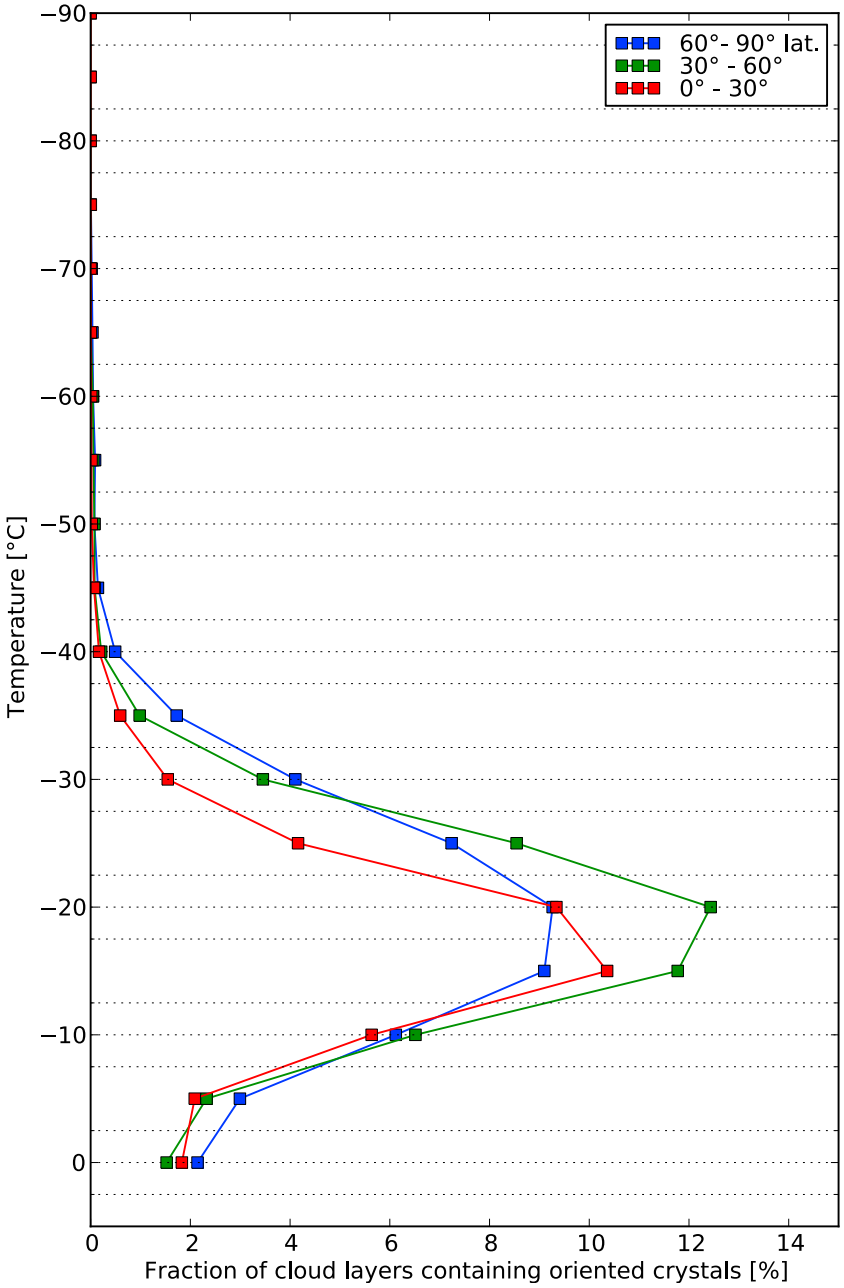


**Figure 3.** Fraction of cloud layers containing oriented crystals as a function of temperature for three bands of latitude. Results are similar for both hemispheres.

coefficients produced by the same particles randomly and horizontally oriented. To the authors' knowledge, it is not possible to retrieve these values for all the CALIOP observations used here from any existing data set, hence we have used theoretical values. Regarding $\delta_r$, *Sassen and Benson* [2001] choose $\delta_r \sim 0.4$ which is common for ice clouds. *Noel and Sassen* [2005] found two values of depolarization ratio for particles susceptible to orientation, which could be used in the present case: $\delta_r \sim 0.25$ for clouds warmer than −20°C and $\delta_r \sim 0.35$ for clouds colder than −30°C; however the number and location of observations were limited, thus it is unclear if these values are representative. In the present case, comparing Figures 1a and 1b shows an noticeable increase in depolarization ratios between 0.3 and 0.4 when switching to a 3° off-nadir angle (section 2.2, lower right arc in Figure 1b); hence a value of $\delta_r \sim 0.35$ was selected for the analysis (in the same range as the previous studies). The theoretical ratio $\frac{\beta_r}{\beta_h}$ was selected as 1/360 following *Sassen and Benson* [2001]. Applying equation (1) on layer-integrated depolarization ratios in layers identified as containing oriented crystals provides a distribution of the fraction of oriented crystals in said clouds. The resulting distributions are very stable with latitude, so only the global distribution is shown (Figure 2). Results show that, in layers where oriented crystals are detected, said crystals constitute a small fraction of the entire population of crystals (generally less than 5%, 2% in average). Since this result is sensitive to the assumptions men-

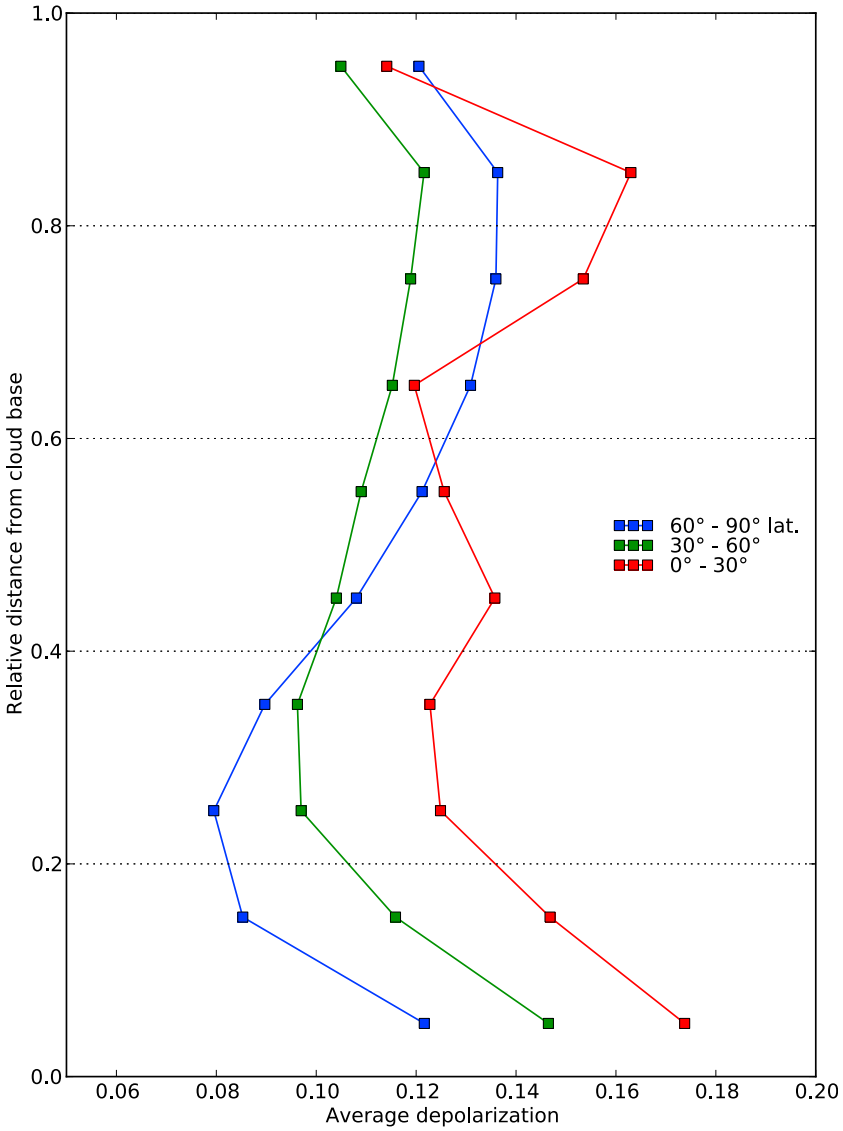


**Figure 4.** Depolarization ratio inside cloud layers containing oriented crystals, as a function of the relative distance from cloud base (0 = cloud base, 1 = cloud top). Results are similar for both hemispheres.

tioned above and based on average optical properties, only the order of magnitude of the oriented fraction should be considered significant, i.e., 1 to 10%.

## 4. Vertical Distribution of Oriented Ice Crystals

### 4.1. Temperature of Cloud Layers Containing Oriented Crystals

[15] For the entire 0.3° off-nadir angle data set, (1) ice cloud layers and (2) ice cloud layers featuring oriented crystals were counted as a function of temperature for three latitude bands. The resulting fraction of cloud layers containing oriented crystals as a function of temperature (Figure 3) shows that oriented crystals are most frequent between −30°C and −10°C, and become rapidly rare out of this temperature range. Since temperature was not used as a criteria in the oriented crystals detection, the robustness of this result suggests that oriented crystals are mostly absent for cloud layers colder than −40°C, and are maximum between −20°C and −10°C. This temperature range is the theoretical domain conducive to the growth of planar crystals [*Thomas et al.*, 1990; *Sassen and Benson*, 2001; *Heymsfield and Miloshevich*, 2003], which have the highest probability of adopting preferential orientation. The fact that oriented crystals are still detected near 0°C could be again due to the resolution mismatch between CALIOP observations and GEOS-5 modeled temperatures fields (section 2.2). The temperature dependence is remarkably similar for all latitudes and seasons, even if the temperature range correlated with crystal orientation spreads toward colder values at high latitudes.

### 4.2. Location of Oriented Crystals Inside the Cloud Layer

[16] In order to evaluate the internal structure of cloud layers containing oriented crystals, profiles of depolarization ratio $\delta$ ($z$) as a function of altitude $z$ were extracted from collocated CALIOP level 1 data (as opposed to the inte-

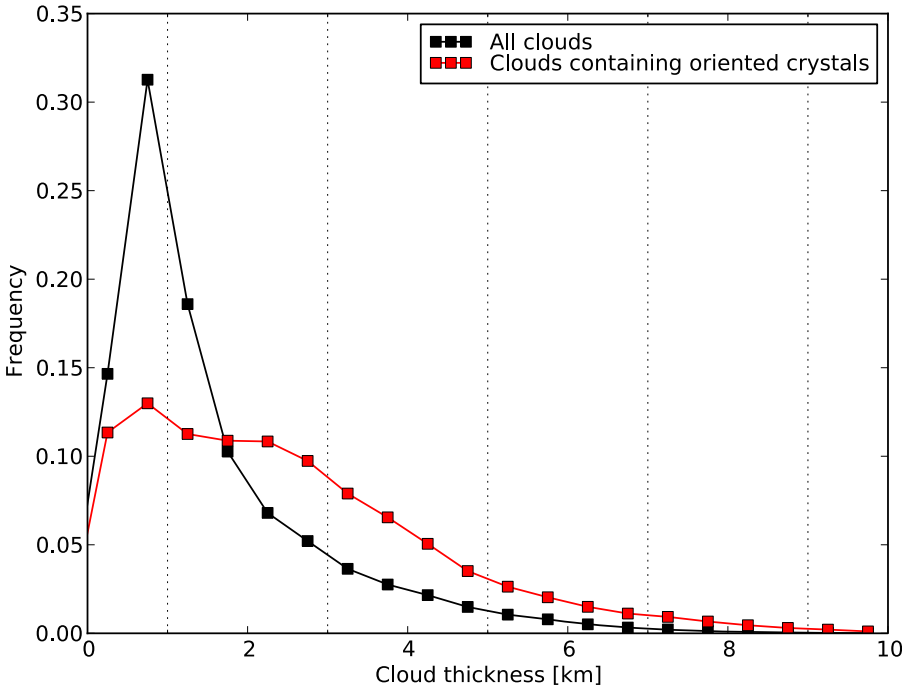


**Figure 5.** Normalized distributions of cloud thickness for all ice clouds and for ice cloud containing oriented crystals.

grated values used so far), averaged horizontally over 5 km to match the resolution of level 2 data, between cloud base $z_b$ and cloud top $z_t$ for layers identified as containing oriented crystals. Depolarization ratios $\delta$ as a function of the relative distance from cloud base $x = \frac{z-z_b}{z_t-z_b}$ (Figure 4) are a minimum right above cloud base ($x \sim 0.2$) for latitudes greater than 30°. Since multiple scattering effects increase during cloud penetration by the lidar beam, and lead to a steady increase in depolarization ratio observed from a spaceborne lidar while approaching cloud base [*Hu et al.*, 2001; *Noel et al.*, 2002], this decrease is most likely underestimated; that is, the minimum should actually be smaller.

[17] This decrease in observed depolarization ratio could be understood as variations in crystal shape, for example, a rounding of ice crystal edges from sublimation during growth in ice-subsaturated regions [*Nelson*, 1998]. Indeed, such effects would be predominantly felt near cloud base. However, in the case of oriented crystals, edge rounding would decrease the quantity of light going through horizontal plane-parallel crystal faces, which would actually increase the depolarization ratio [*Mishchenko et al.*, 1997]. In-layer variability in depolarization ratio can then be understood as a signature of the vertical change in the population of oriented crystals inside the cloud layer; oriented crystals are generally found in the lower half of clouds ($x$ = 0.2 to 0.3 in Figure 4) for latitudes greater than 30°, especially at high latitudes where the frequency of oriented crystals is highest (section 5). Things are different in the tropics, where the depolarization ratio minimum appears to spread out inside the cloud ($0.2 < x < 0.6$). Further analysis reveals that, for layers containing oriented crystals, the cloud thickness distribution is biased toward thick clouds compared to the general ice cloud population (Figure 5). These results suggest that a cloud needs to be thick enough for orientation to take place, which is consistent with the view that crystals only orient themselves once they have reached a certain size, i.e., after sedimentation near the bottom parts of the cloud. The observed oriented crystals could be dendritic or stellar crystals in the early stages of their formation.

## 5. Global-Scale Geographical Distribution of Ice Cloud Layers Containing Oriented Crystals

### 5.1. Global Maps

[18] Since crystal orientation appears strongly dependent on temperature (section 4.1), in the following we will separate ice clouds warmer or colder than −30°C. Top row maps in Figure 6a show the average number of ice cloud layers per profile for all 0.3° off-nadir observations, i.e., the total number of layers detected by CALIOP in a given bin divided by the number of profiles existing in the same bin, for ice clouds colder (Figure 6a, left) or warmer (Figure 6a, right) than −30°C. We show this value instead of the total number of layers in order to remove sampling bias, since CALIOP overpasses more frequently poleward for fixed size lat-lon bins. Overall, ice clouds colder than −30°C are roughly ten times more common than those warmer than −30°C (notice colorbars in Figure 6a). Ice clouds colder than −30°C (Figure 6a, left) are frequent in deeply convective region along the ITCZ (Inter Tropical Convergence Zone): up to 1 layer per profile on average. At midlatitudes the average number of ice cloud layers per profile is a more modest 0.2–0.4. However, this is still more frequent than ice clouds warmer than −30°C (<0.1 layer per profile on average; Figure 6a, right), which are mostly located at higher latitudes and relatively absent of tropical regions. This could be due to frequent optically thick systems in the tropics hiding low-level clouds from CALIOP; however a study of

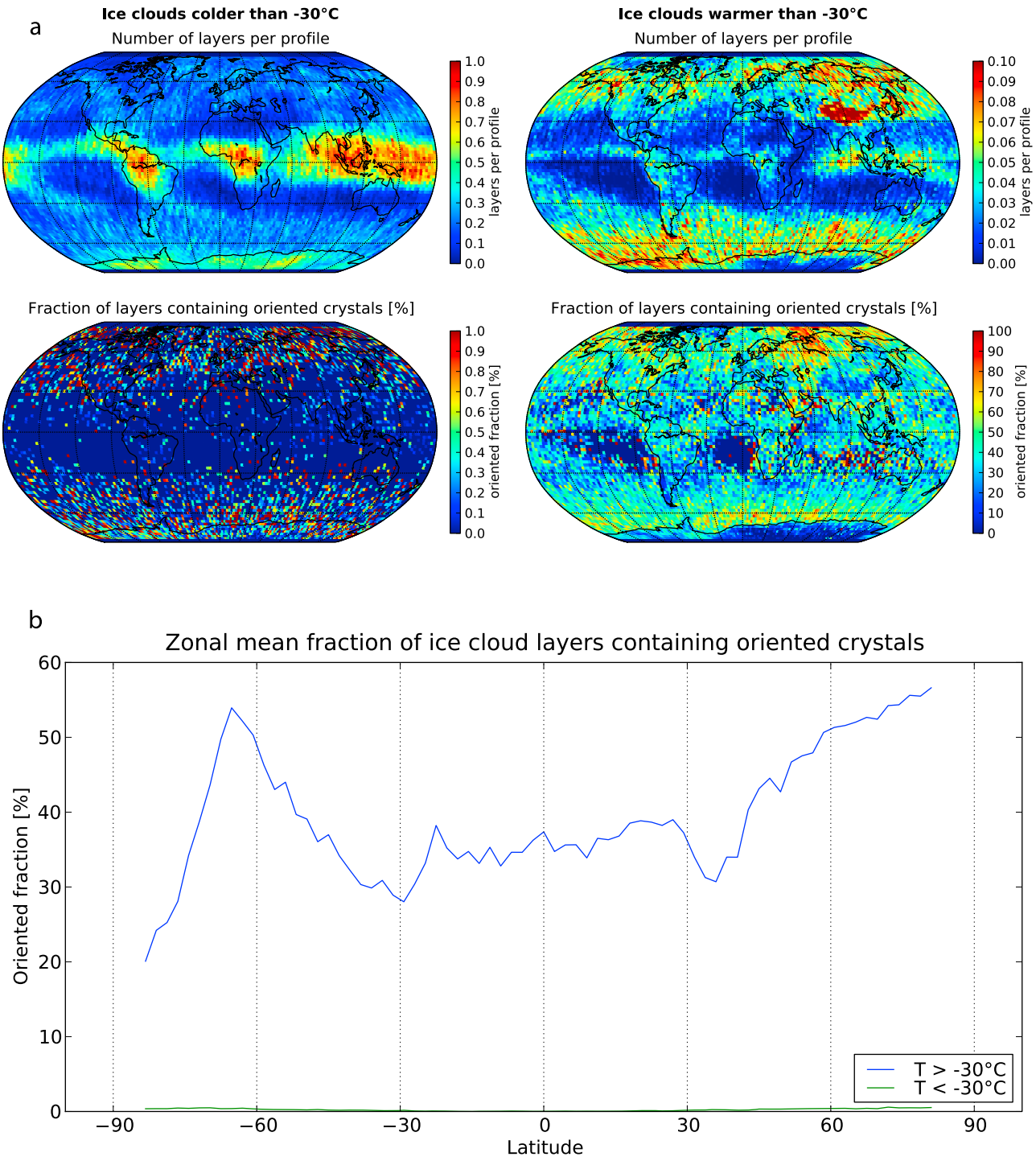


**Figure 6.** (a) (top) Average number of ice cloud layers per profile and (bottom) fraction of these layers identified as containing oriented crystals, considering cloud (left) colder and (right) warmer than −30°C, for 0.3° off-nadir observations (June 2006 to November 2007) in bins of 2.25° × 2.25°. The fraction is defined as the number of layers identified as containing oriented crystals in a bin, divided by the total number of cloud layers in the same bin. (b) Zonal mean fraction of ice clouds layers containing oriented crystals.

CALIOP total extinction altitude in cloudy profiles (using the opacity flag described in section 2.1) revealed that while the sampling coverage decreases at warmer temperatures, it is still above 95% down to the −10°C penetration level.

[19] Focusing now on oriented crystals, the bottom row maps in Figure 6a show the fraction of layers containing oriented crystals for ice clouds colder (Figure 6a, left) or warmer (Figure 6a, right) than −30°C. This oriented fraction

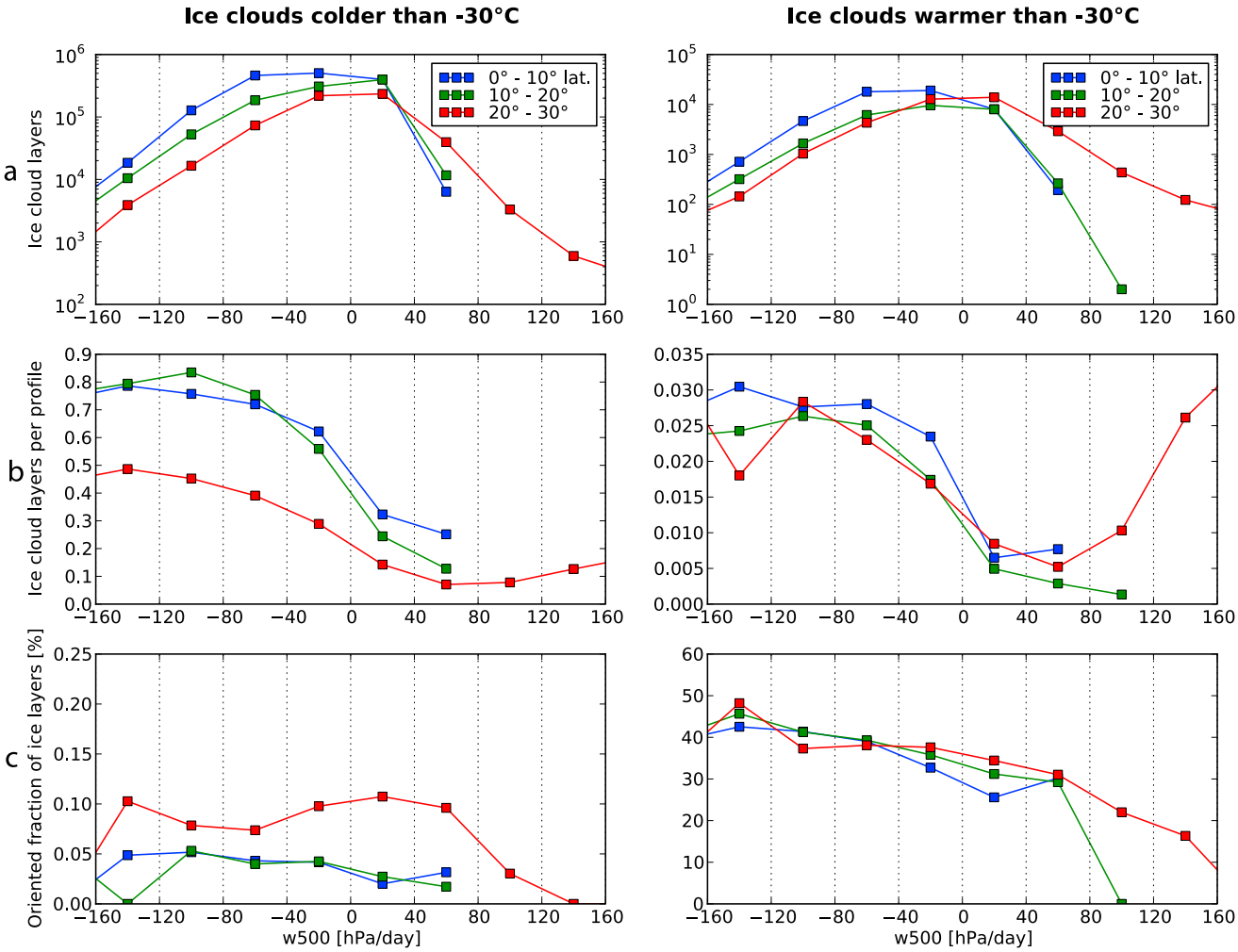


**Figure 7.** (a) Number of ice cloud layers, (b) number of ice cloud layer per profile, and (c) percentage of layers containing oriented crystals as a function of the vertical wind speed at 500 hPa for latitudes below 30° in 0.3° off-nadir observations (June 2006 to November 2007) (left) colder and (right) warmer than −30°C. Results are similar for both hemispheres.

is defined as the number of layers identified as containing oriented crystals in a given bin, divided by the total number of ice clouds layers in the same bin. As found in section 4.1, oriented crystals are extremely rare in ice clouds colder than −30°C; the zonal mean oriented fraction (Figure 6b) increases slightly from near zero at the equator to almost 1% near the poles, but overall appears statistically insignificant. By comparison, oriented crystals appear very common in ice clouds warmer than −30°C; on average they consistently appear in ~35% of those clouds at latitudes between ±30°, this frequency increases over 50% near polar latitudes but drops sharply above Antarctica. Oriented fraction maximum (~90%) is encountered at higher northern latitudes (>60°N) above Siberia (Figure 6a, bottom right). Warm ice clouds are frequent above the Himalaya mountains (Figure 6a, top right) that produce convective orographic clouds, but the oriented fraction is relatively low there (20–30%). Oriented crystals are noticeably absent over the South Atlantic Ocean and the Pacific west of South America, but this might be due to the low number of warm ice clouds collected there. The zonal mean fraction of oriented crystals remains remarkably stable seasonally and quite symmetric around the equator, except for the sharp drop over Antarctica which does not appear in the northern hemisphere.

### 5.2. Link Between Geographic Distribution and Synoptic-Scale Dynamic Indicators

[20] As synoptical-scale dynamics is the first order variable driving the formation of clouds and their properties, we investigated potential correlations between oriented crystals and two indicators of dynamic conditions: the vertical air wind speed in the tropics [*Bony and Dufresne,* 2005] and jet streams speed at midlatitudes.

#### 5.2.1. Tropics

[21] The monthly fraction of cloud layers containing oriented ice crystals was obtained in 2.25° × 2.25° lat-lon bins (as in Figure 6). The fraction in each box was associated to a monthly average of vertical wind speed at 500 hPa (w500) in the same bin, obtained from European Centre for Medium-Range Weather Forecast (ECMWF) reanalysis [*Rabier et al.*, 2000]. This association was done for all months with 0.3° off-nadir observations, for latitudes below

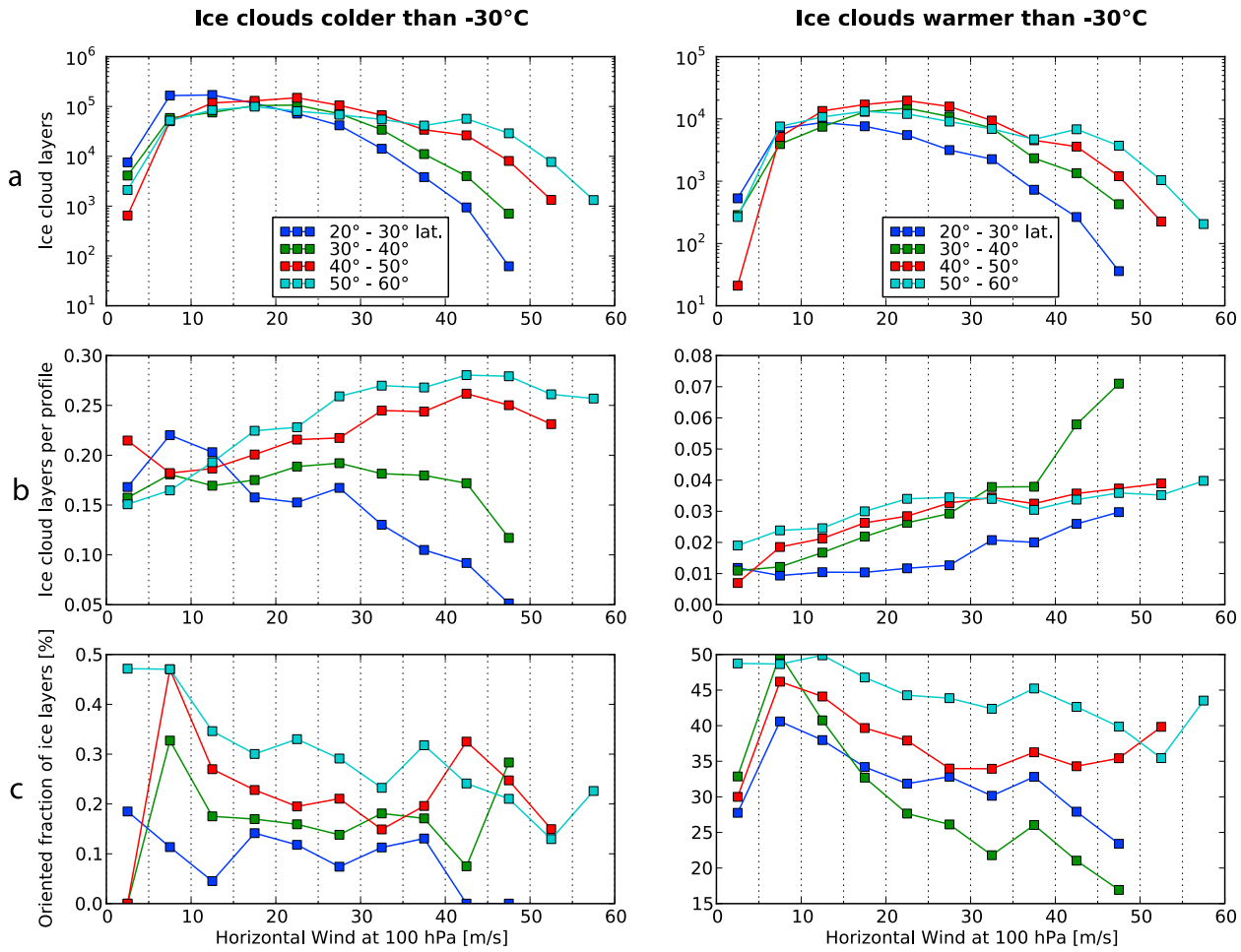


**Figure 8.** (a) Number of ice cloud layers, (b) number of ice cloud layer per profile, and (c) percentage of layers containing oriented crystals as a function of the horizontal wind speed at 100 hPa for latitudes between 20° and 60° in 0.3° off-nadir observations (June 2006 to November 2007) (left) colder and (right) warmer than −30°C. Results are similar for both hemispheres.

30°, and used to derive the average value of oriented crystal fraction as a function of vertical wind speed at 500 hPa. Results are shown for ice clouds colder (Figure 7, left) and warmer (Figure 7, right) than −30°C.

[22] Overall, regions of subsidence (w500 > 0) widely dominate the tropical belt; however, ice clouds are mostly observed in regions of moderate vertical wind speeds between −40 and 40 hPa/day (Figure 7a). Regions of moderate to strong convection (w500 ≪ 0 in Figure 7b) have a considerably higher cloud fraction, meaning that even if they are less frequent they have a higher probability to host ice clouds. As we transition from convection to subsidence (from negative to positive w500), the number of cloud layer per profile drops significantly, although there is a slight increase for strong subsidence regions between 20° and 30° of latitude near the outer edge of the Hadley cell. This last increase is especially noticeable for warm ice clouds (Figure 7b, right). Oriented crystals are very rare in ice clouds colder than −30°C (less than 0.12% of layers), as in section 4.1 and 5.1; their frequency seems unrelated to vertical wind speeds (Figure 7c, left). In warmer ice clouds (Figure 7c, right), oriented crystals are much more frequent (25–50% of layers); significantly more so in regions of convection and less in regions of subsidence. However, it should be kept in mind that strong convection (w500 < −100 hPa/day) or subsidence (w500 > 100 hPa/day) are rare when considering monthly means. In summary, oriented crystals are only frequent in warm ice clouds but those are rare in the tropics; their frequency is higher in regions of convection and lower in regions of subsidence.

### 5.2.2. Mid and High Latitudes

[23] In a similar fashion, the monthly fraction of cloud layers containing oriented crystals in 2.25° × 2.25° lat-lon bins was associated to monthly averages of horizontal wind speed $v_h$ at 100 hPa (near the tropopause, indicator of the presence of jet streams) from ECMWF reanalysis. This association was done for all months with 0.3° off-nadir observations, for latitudes above 30°, and used to derive the oriented crystal fraction as a function of horizontal wind speed at 100 hPa.

[24] In CALIOP observations ice clouds were most often detected at wind speeds below 30 m $s^{-1}$ (Figure 8a). There is a slight increase in detections for wind speeds above 35 m $s^{-1}$ at latitudes above 50°, most probably due to the polar jet; a similar increase is not observed in areas affected by the subtropical jet. Overall, stronger winds are correlated with

an increase in cloud cover at temperatures colder and warmer than −30°C (Figure 8b); an opposite effect is only observed for cold ice clouds at latitudes below 40° (Figure 8b, left). Oriented crystals are slightly more frequent than in the tropics for ice clouds colder than −30°C but are still rare (they appear in less than 0.5% of layers); their frequency seems to roughly decrease with increasing wind speeds (Figure 8c, left) but the trend is not obvious. In warmer ice clouds (Figure 8c, right) oriented crystals are very frequent (15–50%); their frequency drops severely in areas dominated by stronger winds. This effect is especially noticeable at latitudes below 40°, where the subtropical jet is present: there, the oriented crystal frequency drops from ~50% for horizontal winds below 10 m $s^{-1}$ to ~15% for winds near 50 m $s^{-1}$. This drop also appears at other latitudes, but is less noticeable. There is a slight increase in oriented crystal frequency for strong winds (above 50 m $s^{-1}$) at latitudes above 40°, but the number of cloud layers observed in such conditions is relatively small and might not be statistically significant.

[25] Results from this section suggest that synoptic-scale effects have a limited but noticeable correlation with crystal orientation in ice clouds warmer than −30°C: in the tropics, oriented crystals are more frequent in regions of convection; at midlatitudes, oriented crystals are less frequent as horizontal winds speed up.

## 6. Discussion and Conclusion

[26] In this study, we used the optical signature of horizontally oriented crystals in layer-integrated backscatter and depolarization ratio from the CALIOP nadir-looking data set to infer the presence and relative concentration of oriented crystals in clouds on a global scale for 18 continuous months; we investigated correlations between oriented crystals and thermodynamic properties of the atmosphere at local and synoptic scales.

[27] First, oriented crystal appear rarely in the CALIOP data set: ~6% of optically thin ice cloud layers contain oriented crystals; within those layers less than 10% of crystals are oriented (generally 1–5%); that is, the overall oriented crystals ratio in clouds is between $\sim 10^{-3}$ and $\sim 5.10^{-3}$. These findings are very consistent with the most comprehensive to date global-scale studies of oriented crystals based on POLDER-1 observations [*Bréon and Dubrulle*, 2004; *Noel and Chepfer*, 2004]. However, those last analyses consisted of noncontinuous, short observation periods, and required (1) a specific viewing geometry to observe the specular reflection of sunlight and (2) the presence of low-level optically thick clouds to avoid mistaking ocean or land glitter for oriented crystals. As the present results do not share those requirement and describe a longer, continuous timescale, they provide a statistically robust confirmation of previous findings.

[28] Present results have their own limitations however. Depolarization and backscatter can fluctuate within the 5 km resolution of CALIOP level 2 cloud products, thus small-scale cases of oriented crystals could escape the detection. Since these cases should only contain minute amounts of oriented crystals (less than 1%, section 2.2), it seems safe to assume their effects on the cloud radiative impact or lifetime is not significant. More importantly, like all lidar studies, the present analysis cannot be done within opaque clouds (i.e., optical depths roughly above 3); as a consequence those were not considered here and the present results might be biased toward optically thin ice clouds more likely to contain pristine crystals. Optically thick clouds might be underrepresented in the studied data set, including thick tropical systems and mixed-phase clouds containing ice and supercooled liquid layers. The latter appear in ~20% of ice clouds layers between −10°C and −15°C globally [*Hogan et al.*, 2004], i.e., in the temperature range where the present study found the highest concentration of oriented crystals. Recent ground-based observations suggest that supercooled layers play an important part in the formation of planar ice crystals susceptible to orientation [*Westbrook et al.*, 2010], at least at midlatitudes. It is unclear at this point how many supercooled layers appear in the CALIOP data set and how they relate to crystal orientation, as techniques for reliable identification of in-cloud phase variation are still experimental, but it is a question that needs to be addressed.

[29] Among new results, the present study establishes with statistical significance that oriented crystals are almost nonexistent in optically thin ice clouds colder than −30°C; the oriented fraction of those clouds goes from near zero near the equator to 1% at high latitudes near polar circles. Since ice clouds colder than −30°C are a large population, oriented crystals in such clouds are still numerous in absolute terms, as a matter of fact oriented crystals have been identified in cold ice clouds in another study using an approach similar to the one presented here [*Mioche et al.*, 2010]. Considering ice clouds warmer than −30°C, oriented crystals appear in 30 to 50% of them. In those clouds, crystal orientation becomes more frequent with latitude, reaching ~50% above Siberia in the North Hemisphere and above the Ocean just north of Antarctica in the Southern Hemisphere. They appear consistently in ~30% of those clouds in the tropics, a relatively lower frequency probably due to aggregation and riming in convectively produced clouds which leads to irregular crystals [*Heymsfield et al.*, 2002], virtually eliminating the possibility of orientation and specular reflection. Oriented crystals are conspicuously absent in warm ice clouds directly above Antarctica, an observation for which we have no explanation at this point. Analyzing 18 months of data showed that these results are consistently stable with time; the oriented crystals fraction does not seem affected by any seasonal effect.

[30] Crystal orientation appears only remotely correlated with medium and large-scale dynamics (i.e., vertical air speed in the tropics, and jet speed in the extra tropics). Areas dominated with stronger upward movements contain slightly more frequent oriented crystals (Figure 7, section 5.2) than areas dominated by subsidence or weak vertical movements. In a similar way, oriented crystals are observed less in areas influenced by the subtropical and polar jets (Figure 8). Since those correlations are found between monthly averaged values, they cannot be used to infer if a local dynamic state can directly drive or disrupt crystal orientation; previous works [e.g., *Klett*, 1995] provides evidence that turbulence only has a small impact on orientation. It is however possible that local dynamics favor specific particle growth mechanisms, which statistically leads to areas dominated by specific crystal shapes in cirrus more or less susceptible to preferential orientation. In this

regard, the fact that oriented crystals are less frequent in stronger winds (section 5.2) is consistent with observations that planar crystals are less frequent there [*Noel et al.*, 2006].

[31] Most importantly, orientation was shown to be strongly linked with temperature at all latitudes, from the equator to polar regions, all yearlong: oriented crystals were frequently observed in ice clouds warmer than −30°C and almost never in colder ice clouds. This is most certainly due to temperature-dependent crystal growth mechanisms [*Pruppacher and Klett*, 1997] that lead to different crystal shapes more or less prone to orientation at different temperatures. Planar crystal growth occurs predominantly in the −12°C to −18°C range [*Fukuta and Takahashi*, 1999], thus present results reinforce the hypothesis that oriented crystals are mostly planar, with in-cloud vertical motions and sedimentation explaining why oriented crystals are detected in a slightly wider temperature range. The higher detection of oriented crystals just above cloud base requires enhanced planar crystals in that area, which can be explained either by (1) sedimentation from a higher, midcloud supercooled layer where crystals are rapidly nucleated (as described by *Westbrook et al.* [2010]) or (2) ascending air from turbulence near the ice-subsaturated cloud base [*Miloshevich and Heymsfield*, 1997] leading to the nucleation of new pristine ice crystals at colder temperatures higher within the cloud. Future work should investigate the importance of these mechanisms, by (1) studying levels of supersaturation in and around warm and cold ice clouds, which might influence crystal growth and shape [*Spichtinger et al.*, 2004] and (2) correlate supercooled layers with oriented crystals on a global scale. Moreover, *Sassen et al.* [2003] showed the existence of a positive feedback between solar heating and the maintenance of crystal orientation. It might prove fruitful to investigate the global-scale diurnal cycle of crystal orientation by comparing CALIOP daytime and nighttime data.

[32] **Acknowledgments.** The authors would like to thank NASA and CNES for providing the CALIOP data sets used in the present study, the ICARE center for access to said data, and the ClimServ center for the use of its computing facilities. The authors would also like to thank A. Heymsfield and the anonymous reviewers for their useful comments that helped to improve the manuscript.

## References

Beyerle, G., M. Gross, D. Haner, N. Kjome, I. McDermid, T. McGee, J. Rosen, H. J. Schafer, and O. Schrems (2001), A lidar and backscatter sonde measurement campaign at Table Mountain during February–March 1997: Observations of cirrus clouds, *J. Atmos. Sci.*, *58*, 1275–1287, doi:10.1175/1520-0469(2001)058<1275:ALABSM>2.0.CO;2.

Bogdan, A., M. J. Molina, K. Sassen, and M. Kulmala (2006), Formation of low-temperature cirrus from $H_2SO_4/H_2O$ aerosol droplets, *J. Phys. Chem. A.*, *110*, 12,541–12,542, doi:10.1021/jp065898e.

Bony, S., and J.-L. Dufresne (2005), Marine boundary layer clouds at the heart of tropical cloud feedback uncertainties in climate models, *Geophys. Res. Lett.*, *32*, L20806, doi:10.1029/2005GL023851.

Bréon, F. M., and B. Dubrulle (2004), Horizontally oriented plates in clouds, *J. Atmos. Sci.*, *61*, 2888–2898, doi:10.1175/JAS-3309.1.

Chepfer, H., and V. Noel (2009), A tropical "NAT-like" belt observed from space, *Geophys. Res. Lett.*, *36*, L03813, doi:10.1029/2008GL036289.

Chepfer, H., G. Brogniez, P. Goloub, F. M. Breon, and P. Flamant (1999), Observations of horizontally oriented ice crystals in cirrus clouds with POLDER-1/ADEOS-1, *J. Quant. Spectrosc. Radiat. Transfer*, *63*, 521–543, doi:10.1016/S0022-4073(99)00036-9.

Cho, H. M., P. Yang, G. Kattawar, S. Nasiri, Y. Hu, P. Minnis, C. Trepte, and D. Winker (2008), Depolarization ratio and attenuated backscatter for nine cloud types: Analyses based on collocated CALIPSO lidar and MODIS measurements, *Opt. Express*, *16*(6), 3931–3948, doi:10.1364/OE.16.003931.

Evans, K., S. Walter, A. Heymsfield, and M. Deeter (1998), Modeling of submillimeter passive remote sensing of cirrus clouds, *J. Appl. Meteorol.*, *37*, 184–205, doi:10.1175/1520-0450(1998)037<0184:MOSPRS>2.0.CO;2.

Fukuta, N., and T. Takahashi (1999), The growth of atmospheric ice crystals: A summary of findings in vertical supercooled cloud tunnel studies, *J. Atmos. Sci.*, *56*, 1963–1979, doi:10.1175/1520-0469(1999)056<1963:TGOAIC>2.0.CO;2.

Heymsfield, A., and J. Iaquinta (2000), Cirrus crystal terminal velocity, *J. Atmos. Sci.*, *57*, 916–938, doi:10.1175/1520-0469(2000)057<0916:CCTV>2.0.CO;2.

Heymsfield, A., and L. Miloshevich (2003), Parameterizations for the cross-sectional area and extinction of cirrus and stratiform ice cloud particles, *J. Atmos. Sci.*, *60*, 936–956, doi:10.1175/1520-0469(2003)060<0936:PFTCSA>2.0.CO;2.

Heymsfield, A., A. Bansemer, P. Field, S. Durden, J. Stith, J. Dye, W. Hall, and C. Grainger (2002), Observations and parameterization of particle size distribution in deep tropical cirrus and stratiform precipitating clouds: Results from in situ observations in TRMM field campaigns, *J. Atmos. Sci.*, *59*, 3457–3491, doi:10.1175/1520-0469(2002)059<3457:OAPOPS>2.0.CO;2.

Hogan, R. J., M. D. Behera, E. J. O'Connor, and A. J. Illingworth (2004), Estimate of the global distribution of stratiform supercooled liquid water clouds using the LITE lidar, *Geophys. Res. Lett.*, *31*, L05106, doi:10.1029/2003GL018977.

Hu, Y., D. Winker, P. Yang, B. Baum, L. Poole, and L. Vann (2001), Identification of cloud phase from PICASSO-CENA lidar depolarization: A multiple scattering sensitivity study, *J. Quant. Spectrosc. Radiat. Transfer*, *70*, 569–579, doi:10.1016/S0022-4073(01)00030-9.

Hu, Y., et al. (2007), The depolarization–attenuated backscatter relation: CALIPSO lidar measurements vs. theory, *Opt. Express*, *15*(9), 5327–5332, doi:10.1364/OE.15.005327.

Hu, Y., et al. (2009), CALIPSO/CALIOP cloud phase discrimination algorithm, *J. Atmos. Oceanic Technol.*, *26*, 2293–2309, doi:10.1175/2009JTECHA1280.1.

Immler, F., R. Treffeisen, D. Engelbart, K. Krüger, and O. Schrems (2008), Cirrus, contrails, and ice supersaturated regions in high pressure systems at northern mid latitudes, *Atmos. Chem. Phys.*, *8*, 1689–1699.

Klett, J. (1995), Orientation model for particles in turbulence, *J. Atmos. Sci.*, *52*, 2276–2285, doi:10.1175/1520-0469(1995)052<2276:OMFPIT>2.0.CO;2.

Lavigne, C., A. Roblin, and P. Chervet (2008), Solar glint from oriented crystals in cirrus clouds, *Appl. Opt.*, *47*, 6266–6276, doi:10.1364/AO.47.006266.

Liu, Z., A. H. Omar, Y. Hu, M. A. Vaughan, and D. M. Winker (2005), CALIOP algorithm basis document-Part 3: Scene classification algorithms, technical report, Langley Res. Cent., Hampton, Va.

Lynch, D., S. Gedzelman, and A. Fraser (1994), Subsuns, Bottlinger's rings and elliptical halos, *Appl. Opt.*, *33*, 4580–4589, doi:10.1364/AO.33.004580.

Masuda, K., and H. Ishimoto (2004), Influence of particle orientation on retrieving cirrus cloud properties by use of total and polarized reflectances from satellite measurements, *J. Quant. Spectrosc. Radiat. Transfer*, *85*, 183–193.

Miloshevich, L. M., and A. J. Heymsfield (1997), A balloon-borne continuous cloud particle replicator for measuring vertical profiles of cloud microphysical properties: Instrument design, performance, and collection efficiency analysis, *J. Atmos. Oceanic Technol.*, *14*, 753–768, doi:10.1175/1520-0426(1997)014<0753:ABBCCP>2.0.CO;2.

Mioche, G., D. Josset, J.-F. Gayet, J. Pelon, A. Garnier, A. Minikin, and A. Schwarzenboeck (2010), Validation of the CALIPSO/CALIOP extinction coefficients from in situ observations in mid-latitude cirrus clouds during CIRCLE-2 experiment, *J. Geophys. Res.*, doi:10.1029/2009JD012376, in press.

Mishchenko, M., D. Wielaard, and B. Carlson (1997), T-matrix computations of zenith-enhanced lidar backscatter from horizontally oriented ice plates, *Geophys. Res. Lett.*, *24*, 771–774, doi:10.1029/97GL00545.

Nelson, J. (1998), Sublimation of ice crystals, *J. Atmos. Sci.*, *55*, 910–919, doi:10.1175/1520-0469(1998)055<0910:SOIC>2.0.CO;2.

Noel, V., and H. Chepfer (2004), Study of ice crystal orientation in cirrus clouds based on satellite polarized radiance measurements, *J. Atmos. Sci.*, *61*, 2073–2081, doi:10.1175/1520-0469(2004)061<2073:SOICOI>2.0.CO;2.

Noel, V., and K. Sassen (2005), Study of planar ice crystal orientations in ice clouds from scanning polarization lidar observations, *J. Appl. Meteorol.*, *44*, 653–664, doi:10.1175/JAM2223.1.

Noel, V., G. Roy, L. Bissonnette, H. Chepfer, and P. Flamant (2002), Analysis of lidar measurements of ice clouds at multiple incidence angles, *Geophys. Res. Lett.*, *29*(9), 1338, doi:10.1029/2002GL014828.

Noel, V., H. Chepfer, M. Haeffelin, and Y. Morille (2006), Classification of ice crystal shapes in midlatitude ice clouds from three years of lidar observations over the SIRTA observatory, *J. Atmos. Sci.*, *63*, 2978–2991, doi:10.1175/JAS3767.1.

Noel, V., A. Hertzog, H. Chepfer, and D. Winker (2008), Polar stratospheric clouds over Antarctica from the CALIPSO spaceborne lidar, *J. Geophys. Res.*, *113*, D02205, doi:10.1029/2007JD008616.

Noel, V., A. Hertzog, and H. Chepfer (2009), CALIPSO observations of wave-induced PSCs with near-unity optical depth over Antarctica in 2006–2007, *J. Geophys. Res.*, *114*, D05202, doi:10.1029/2008JD010604.

Pitts, M., L. Thomason, L. Poole, and D. Winker (2007), Characterization of polar stratospheric clouds with spaceborne lidar: CALIPSO and the 2006 Antarctic season, *Atmos. Chem. Phys.*, *7*, 5207–5228.

Platt, C. M. R., N. Abshire, and G. McNice (1978), Some microphysical properties of an ice cloud from lidar observations of horizontally oriented crystals, *J. Appl. Meteorol.*, *17*, 1220–1224, doi:10.1175/1520-0450(1978)017<1220:SMPOAI>2.0.CO;2.

Prigent, C., E. Defer, J. Pardo, C. Pearl, W. B. Rossow, and J. Pinty (2005), Relations of polarized scattering signatures observed by the TRMM Microwave Instrument with electrical processes in cloud systems, *Geophys. Res. Lett.*, *32*, L04810, doi:10.1029/2004GL022225.

Pruppacher, H. R., and J. D. Klett (1997), *Microphysics of Clouds and Precipitation*, *Atmos. Oceanogr. Sci. Libr.*, vol. 914, Kluwer Acad., Norwell, Mass.

Rabier, F., H. Jrvinen, E. Klinker, J. F. Mahfouf, and A. Simmons (2000), The ECMWF operational implementation of four dimensional variational assimilation. I: Experimental results with simplified physics, *Q. J. R. Meteorol. Soc.*, *126*, 1143–1170, doi:10.1256/smsqj.56414.

Sassen, K. (1980), Remote sensing of planar ice crystals fall attitude, *J. Meteorol. Soc. Jpn.*, *58*, 422–433.

Sassen, K., and S. Benson (2001), A midlatitude Cirrus cloud climatology from the facility for atmospheric remote sensing. Part II: Microphysical properties derived from lidar depolarisation, *J. Atmos. Sci.*, *58*, 2103–2111, doi:10.1175/1520-0469(2001)058<2103:AMCCCF>2.0.CO;2.

Sassen, K., and Y. Takano (2000), Parry arc: A polarization lidar, ray-tracing, and aircraft case study, *Appl. Opt.*, *39*, 6738–6745, doi:10.1364/AO.39.006738.

Sassen, K., K. Liou, Y. Takano, and V. Khvorostyanov (2003), Diurnal effects in the composition of cirrus clouds, *Geophys. Res. Lett.*, *30*(10), 1539, doi:10.1029/2003GL017034.

Spichtinger, P., and K. M. Gierens (2009), Modelling of cirrus clouds - Part 1b: Structuring cirrus clouds by dynamics, *Atmos. Chem. Phys.*, *9*, 707–719.

Spichtinger, P., K. Gierens, H. Smith, J. Ovarlez, and J. Gayet (2004), On the distribution of relative humidity in cirrus clouds, *Atmos. Chem. Phys.*, *4*, 639–647.

Takano, Y., and K. Liou (1989), Solar radiative transfer in cirrus clouds. Part II: Theory and computation of multiple scattering in an anisotropic medium, *J. Atmos. Sci.*, *46*, 20–36, doi:10.1175/1520-0469(1989)046<0020:SRTICC>2.0.CO;2.

Thomas, L., J. Cartwright, and D. Wareing (1990), Lidar observations of the horizontal orientation of ice crystals in cirrus clouds, *Tellus, Ser. B*, *42*, 211–216.

Vaughan, M. A., S. Young, D. M. Winker, K. Powell, A. Omar, Z. Liu, Y. Hu, and C. Hostetler (2004), Fully automated analysis of space-based lidar data: An overview of the CALIPSO retrieval algorithms and data products, *Proc. SPIE Int. Soc. Opt. Eng.*, *5575*, 16–30, doi:10.1117/12.572024.

Vaughan, M. A., D. M. Winker, and K. Powell (2005), CALIOP algorithm basis document-Part 2: Feature detection and layer properties algorithms, *PC-SCI-202 Part 2*, Langley Research Center, Hampton, Va.

Westbrook, C. D. (2008), The fall speeds of sub-100$\mu$m ice crystals, *Q. J. R. Meteorol. Soc.*, *134*, 1243–1251, doi:10.1002/qj.290.

Westbrook, C. D., A. J. Illingworth, E. J. O'Connor, and R. J. Hogan (2010), Doppler lidar measurements of oriented planar ice crystals falling from supercooled and glaciated layer clouds, *Q. J. R. Meteorol. Soc.*, *136*, 260–276.

Winker, D., W. Hunt, and M. McGill (2007), Initial performance assessment of CALIOP, *Geophys. Res. Lett.*, *34*, L19803, doi:10.1029/2007GL030135.

Yang, P., X. Yong, D. Winker, J. Zhao, C. Hostetler, L. Poole, B. Baum, M. Mishchenko, and J. Reichardt (2003), Enhanced lidar backscattering by quasi-horizontally oriented ice crystals plates in cirrus clouds, *J. Quant. Spectrosc. Radiat. Transfer*, *79*, 1139–1157.

H. Chepfer, Laboratoire de Météorologie Dynamique, IPSL, Université Paris 6, F-75252 Paris, France.

V. Noel, Laboratoire de Météorologie Dynamique, IPSL, Ecole Polytechnique, CNRS, F-91128 Palaiseau, France. (vincent.noel@lmd.polytechnique.fr)